Hydrogen Atoms under Magnification: Direct Observation of the Nodal Structure of Stark States

A. S. Stodolna,[1,*] A. Rouzée,[1,2] F. Lépine,[3] S. Cohen,[4] F. Robicheaux,[5] A. Gijsbertsen,[1] J. H. Jungmann,[1] C. Bordas,[3] and M. J. J. Vrakking[1,2,*]

[1]*FOM Institute AMOLF, Science Park 104, 1098 XG Amsterdam, Netherlands*
[2]*Max-Born-Institut, Max Born Straße 2A, D-12489 Berlin, Germany*
[3]*Institut Lumière Matière, Université Lyon 1, CNRS, UMR 5306, 10 Rue Ada Byron, 69622 Villeurbanne Cedex, France*
[4]*Atomic and Molecular Physics Laboratory, Physics Department, University of Ioannina, 45110 Ioannina, Greece*
[5]*Department of Physics, Auburn University, Auburn, Alabama 36849, USA*

(Received 18 January 2013; revised manuscript received 13 March 2013; published 20 May 2013)

To describe the microscopic properties of matter, quantum mechanics uses wave functions, whose structure and time dependence is governed by the Schrödinger equation. In atoms the charge distributions described by the wave function are rarely observed. The hydrogen atom is unique, since it only has one electron and, in a dc electric field, the Stark Hamiltonian is exactly separable in terms of parabolic coordinates (η, ξ, φ). As a result, the microscopic wave function along the ξ coordinate that exists in the vicinity of the atom, and the projection of the continuum wave function measured at a macroscopic distance, share the same nodal structure. In this Letter, we report photoionization microscopy experiments where this nodal structure is directly observed. The experiments provide a validation of theoretical predictions that have been made over the last three decades.

DOI: 10.1103/PhysRevLett.110.213001 PACS numbers: 32.80.Fb, 32.60.+i

The development of quantum mechanics in the early part of the last century has had a profound influence on the way that scientists understand the world. Central to quantum mechanics is the concept of a wave function that satisfies the time-dependent Schrödinger equation [1]. According to the Copenhagen interpretation, the wave function describes the probability of observing the outcome of measurements on a quantum mechanical system, such as measurements of the energy or the position or momenta of constituents [2]. The Copenhagen interpretation thus allows reconciling the occurrence of nonclassical phenomena on the nanoscale with manifestations and observations made on the macroscale, which correspond to viewing one of a number of possible realizations allowed for by the wave function.

Despite the overwhelming impact on modern electronics and photonics, understanding quantum mechanics and the many possibilities that it describes continues to be intellectually challenging, and has motivated numerous experiments that illustrate the intriguing predictions contained in the theory [3]. Using ultrafast lasers, Rydberg wave packet experiments have been performed illustrating how coherent superpositions of quantum mechanical stationary states describe electrons that move on periodic orbits around nuclei [4]. The wave function of each of these electronic stationary states is a standing wave, with a nodal pattern that reflects the quantum numbers of the state. Mapping of atomic and molecular momentum wave functions has been extensively explored by means of (e, $2e$) spectroscopy, using coincident detection of the momentum of both an ejected and a scattered electron to retrieve the momentum distribution of the former prior to ionization [5]. In the spirit of scanning tunneling methods, orbital tomography based on high harmonic generation was developed as a method allowing the determination of atomic and molecular orbitals [6,7]. In this Letter we will present experiments where the nodal structure of electronic wave functions of hydrogen atoms is measured, making use of a photoionization microscopy experiment, where photoelectrons resulting from ionization after excitation of a quasibound Stark state are measured on a two-dimensional detector.

The hydrogen is a unique atom, since it only has one electron and, in a dc electric field, the Stark Hamiltonian is exactly separable in terms of parabolic coordinates. For this reason, an experimental method was proposed about thirty years ago, when it was suggested that experiments ought to be performed projecting low-energy photoelectrons resulting from the ionization of hydrogen atoms onto a position-sensitive two-dimensional detector placed perpendicularly to the static electric field, thereby allowing the experimental measurement of interference patterns directly reflecting the nodal structure of the quasibound atomic wave function [8–10].

In a static electric field F the wave function of atomic hydrogen can be separated in terms of the parabolic coordinates η, ξ, φ ($\eta = r - z$ and $\xi = r + z$, where r is the distance of the electron from the proton, z is the displacement along the electric field axis and $\varphi = \tan^{-1}(y/x)$ is the azimuthal angle [see Fig. 1(a) and Ref. [11]]). Note that atomic units are used, unless specified otherwise. Consequently, the wave function may be written as a product of functions $\chi_1(\xi)$ and $\chi_2(\eta)$ that separately describe the dependence along ξ and η,

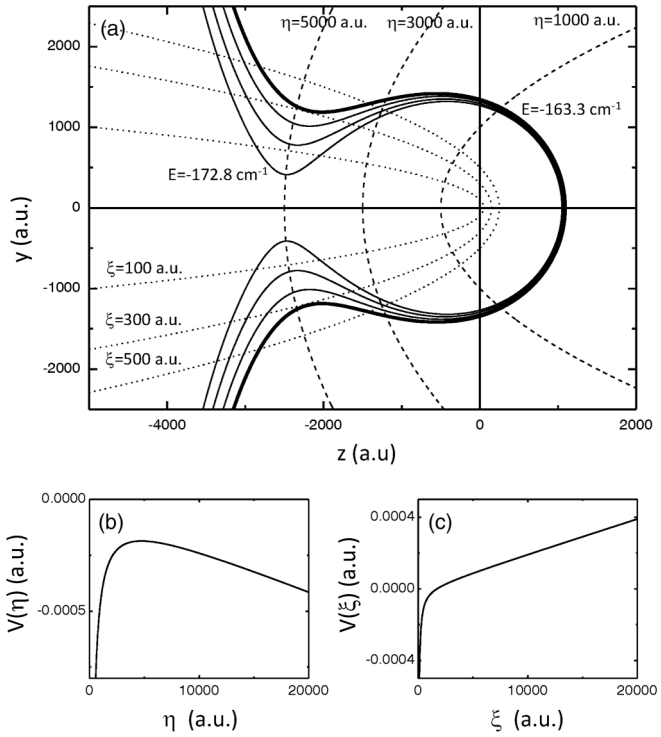

FIG. 1. (a) Potential energy landscape and relevant coordinate system for hydrogen atom photoionization microscopy in an 808 V/cm electric field (a.u. = atomic units). The hydrogen atom sits at the origin of the (z, y) coordinate system and the electric field is along the z axis. The boundary between the classically allowed and the classically forbidden region is plotted (solid lines) at the excitation energies of the four measurements that are shown in Fig. 3, i.e., ranging from $E = -172.8$ cm^{-1} to $E = -163.3$ cm^{-1} (thick outer solid line). Close to the saddle point, the electron can only escape through a very narrow gap in the Coulomb + dc field potential. The parabolic coordinates $\eta = r - z$ and $\xi = r + z$ are illustrated by plotting a series of contours at constant η (dashed lines) and ξ (dotted lines). The electron motion is always bound in the ξ coordinate whereas the motion along the η coordinate depends on the energy available for the η motion; (b) and (c) Potential energy curves $V(\eta) = -\frac{Z_2}{2\eta} + \frac{m^2-1}{8\eta^2} - \frac{F\eta}{8}$ and $V(\xi) = -\frac{Z_1}{2\xi} + \frac{m^2-1}{8\xi^2} + \frac{F\xi}{8}$, describing the motion along the η and ξ coordinates [11], where $Z_1 = (n_1 + \frac{|m|+1}{2})/n$ and $Z_2 = (n_2 + \frac{|m|+1}{2})/n$. $V(\eta)$ and $V(\xi)$ are shown for the $(n_1, n_2, m) = (3, 26, 0)$ quasibound state at $E = -163.3$ cm^{-1}.

i.e., $\Psi(\xi, \eta, \varphi) = (2\pi\eta\xi)^{-1/2}\chi_1(\xi)\chi_2(\eta)e^{im\varphi}$. The functions $\chi_1(\xi)$ and $\chi_2(\eta)$ satisfy the ordinary differential equations,

$$\frac{d^2\chi_1}{d\xi^2} + \left(\frac{E}{2} + \frac{Z_1}{\xi} - \frac{m^2-1}{4\xi^2} - \frac{1}{4}F\xi\right)\chi_1 = 0,$$
$$\frac{d^2\chi_2}{d\eta^2} + \left(\frac{E}{2} + \frac{Z_2}{\eta} - \frac{m^2-1}{4\eta^2} + \frac{1}{4}F\eta\right)\chi_2 = 0.$$

In these expressions m is the magnetic quantum number and Z_1 and Z_2 are separation constants subject to the condition $Z_1 + Z_2 = 1$. The parabolic quantum numbers n_1 and n_2 are related to the principal quantum number via $n = n_1 + n_2 + |m| + 1$. Functions $\chi_1(\xi)$ and $\chi_2(\eta)$ have n_1 and n_2 nodes along the ξ and η coordinates, respectively. Figure 1(a) shows the potential energy landscape for the hydrogen atom in an 808 V/cm electric field. The electron motion is always bound in the ξ coordinate whereas the motion along the η coordinate depends on the energy available for its motion. Figures in the lower panels illustrate the potential energy curves $V(\eta) = -\frac{Z_2}{2\eta} + \frac{m^2-1}{8\eta^2} - \frac{F\eta}{8}$ and $V(\xi) = -\frac{Z_1}{2\xi} + \frac{m^2-1}{8\xi^2} + \frac{F\xi}{8}$ (please note that in the literature other conventions for the definition of $V(\eta)$ and $V(\xi)$ are in use as well; see, e.g., Ref. [12]), defining the motion along the η and ξ coordinates, respectively. Reference [8] contained a remarkable prediction for the special case where the atomic hydrogen photoionization involves the excitation of quasibound Stark states. In this case, where both n_1 and n_2 are good quantum numbers and the electron tunnels through the barrier in the potential energy curve associated with the η coordinate, the measurements should show a total of n_1 dark fringes, directly revealing an important signature of the Stark state involved. However, to date, this experiment was never performed.

Motivated by the theoretical predictions for the configuration of the above-mentioned "photoionization microscope" [8], a photodetachment microscope for negative ions was first constructed by Blondel *et al.* [13]. Their experiments clearly revealed interferences between the photoelectrons en route to the detector, in agreement with simple semiclassical considerations by Du [14]. In photodetachment, the photoelectrons follow one of two possible parabolic trajectories to the two-dimensional detector. By contrast, in a photoionization experiment that starts from a neutral sample, the photoelectrons move in a combined static electric + Coulomb field, significantly complicating the dynamics and leading to the existence of an infinite number of trajectories that the photoelectron can follow to the detector [15].

Given the considerable challenges connected to the experimental use of atomic hydrogen, first attempts to implement photoionization microscopy were performed on Xe atoms by Nicole et al. [16]. Observed interference rings were interpreted in the framework of a semiclassical treatment [17], excluding the possibility of resonant excitation of a Stark state. The experiments themselves were performed both with and without the resonant excitation of quasibound Stark states, and no significant differences were observed [18]. More recently, photoionization microscopy experiments were performed for Li atoms [19], revealing first indications of differences in the radial distributions for on- and off-resonance excitation. This work provides the motivation for the hydrogen experiments reported in the present Letter, where we present results for both resonant and nonresonant ionization, and where

we convincingly validate the long time predictions of Demkov *et al.* [8,9].

An atomic hydrogen beam was formed by collimating hydrogen atoms resulting from the photodissociation of H_2S gas in a first vacuum chamber (see Fig. 2 and the Supplemental Material [20]). The hydrogen atoms were ionized in the active region of a velocity map imaging (VMI) spectrometer [21], where an 808 V/cm static electric field was applied. The atoms were resonantly excited to a mixture of $n = 2$ s and p states by a two-photon transition ($\lambda_{\text{laser}} = 243$ nm) and were ionized using narrowband, tunable laser pulses ($\lambda_{\text{laser}} = 365$–$367$ nm, $\tau_{\text{laser}} = 8$ ns) from a Fourier-limited, home-built pulsed dye amplifier [22]. The polarization of the 365–367 nm laser was along the static electric field (i.e., perpendicular to the detector). A dual microchannel plate (MCP) detector followed by a phosphor screen and a CCD camera was used to record the photoelectrons. An electrostatic zoom lens magnified the images by about 1 order of magnitude compared to the size that would have been measured without this lens [23].

The main results of the experiments are shown in Fig. 3. In this figure calculated and experimental results are shown for four experiments, where the hydrogen atoms were excited to the $(n_1, n_2, m) = (0, 29, 0), (1, 28, 0), (2, 27, 0)$ and $(3, 26, 0)$ quasibound Stark states. As indicated in Fig. 3, the states lie at energies of -172.82 cm^{-1}, -169.67 cm^{-1}, -166.45 cm^{-1}, and -163.30 cm^{-1} with respect to the field-free ionization limit, i.e., just above the saddle point in the Coulomb + dc field potential, which lies at -174.00 cm^{-1}. According to Eq. (6) of Ref. [24], the validity of which was checked experimentally [25], the ionization rate of these states covered a range from $\Gamma = 2.2 \times 10^{10}$ s^{-1} to $\Gamma = 7.25 \times 10^{9}$ s^{-1}, which [using $\delta E(\text{cm}^{-1}) = 5.3 \times 10^{-12}\ \Gamma(\text{s}^{-1})$] implies line widths comparable to the 0.005 cm^{-1} bandwidth of our excitation laser. These states could readily be identified in wavelength scans, since the ionization is complete before the hydrogen atoms leave the interaction region of the VMI [26]. By contrast, in the same energy range Stark states in the $n = 31$ manifold ($\Gamma > 10^{12}$ s^{-1}) lead to very broad resonances, while states in the $n = 29$ manifold ($\Gamma < 10^{6}$ s^{-1}) undergo insufficient ionization before the atoms fly out of the interaction region. Total ionization spectra as a function of excitation energy in the given static electric field were successfully reproduced by means of the semiclassical Stark theory of Harmin [27,28]. The parabolic quantum number n_1 was identified by comparing the experimental spectra with separate theoretical excitation curves for

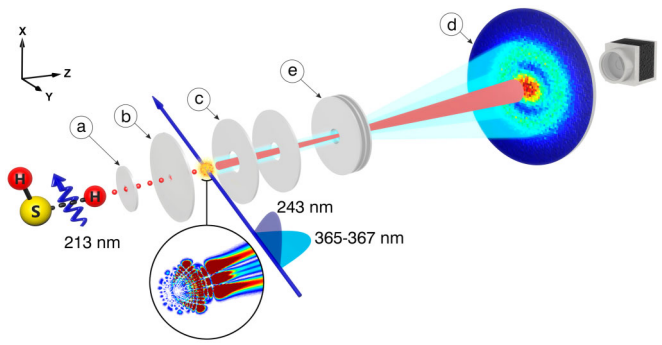

FIG. 2 (color online). Schematic overview of the experiment. An atomic hydrogen beam was formed by photodissociating H_2S and placing a 3 mm aperture (a) 65 mm downstream. In the active region of a velocity map imaging (VMI) spectrometer, the ground state hydrogen atoms were first excited to a mixture of $n = 2$ s and p states by a two-photon transition using a pulsed 243 nm laser. Next, they were ionized by a Fourier-limited, tunable (365–367 nm), UV laser. By applying a voltage difference across the repeller (b) and extractor (c) electrodes, the photoelectrons were accelerated towards a two-dimensional detector (d), consisting of a set of microchannel plates (MCPs), a phosphor screen and a CCD camera. En route to the MCP detector, the photoelectrons passed through a three-element Einzel lens (e), allowing an increase of the diameter of the recorded image by about one order of magnitude.

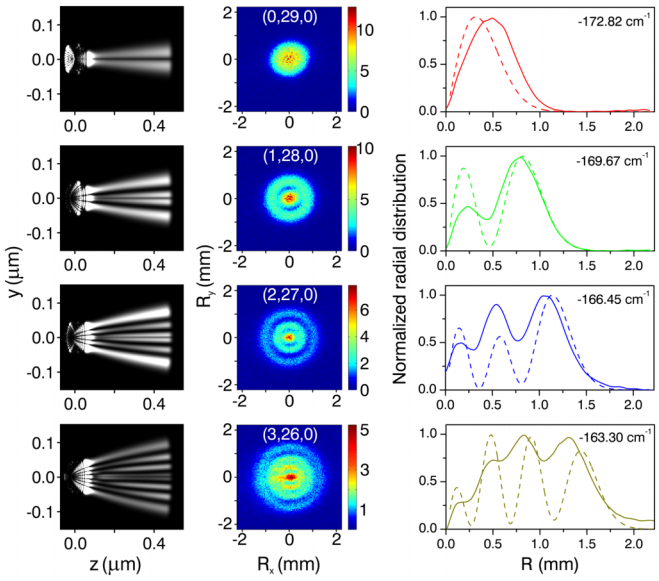

FIG. 3 (color online). Experimental observation of the transverse nodal structure of four atomic hydrogen Stark states. The images in the middle show experimental measurements for $(n_1, n_2, m) = (0, 29, 0)$, $(1, 28, 0)$, $(2, 27, 0)$, and $(3, 26, 0)$. Interference patterns are clearly observed where the number of nodes corresponds to the value of n_1. The results may be compared to TDSE calculations shown to the left (for details see text), revealing that the experimentally observed nodal structures originate from the transverse nodal structure of the initial state that is formed upon laser excitation. A comparison of the experimentally measured (solid lines) and calculated radial (dashed lines) probability distributions $P(R)$ is shown to the right of the experimental results. In order to make this comparison, the computational results were scaled to the macroscopic dimensions of the experiment. Please note that, since $P(R) = \int P(R, \alpha) R d\alpha$, the radial probability distributions $P(R)$ have a zero at $R = 0$, even if the two-dimensional images $P(R, \alpha)$ do not.

each n_1 channel. Given the value of n_1, the value of n_2 was subsequently determined by applying the Wentzel-Kramers-Brillouin quantization rule along the η coordinate.

The main result of the experiment, which is directly visible in the four images shown in the middle of Fig. 3, is the observation of an interference pattern with a number of dark fringes corresponding to the value of n_1. This observation validates the prediction by Demkov and coworkers [8,9] and illustrates that photoionization microscopy can be used to visualize the nodal structure of $\chi_1(\xi)$ for quasibound Stark states of the hydrogen atom. A rationalization for this behavior can be found in the calculations shown to the left of the experimental images. Here, results of propagating the time-dependent Schrödinger equation (TDSE; see the Supplemental Material [20]) following excitation of the hydrogen atom at the energies used in the experiments are shown [29]. The graphs represent time-integrated plots of the two-dimensional electron density $\rho(r, z) = r|\Psi(r, t)|^2$, evaluated from the time of excitation ($t = 0$) to a time delay of 600 ps. The nodal structure that is observable at a large distance from the proton (here, 0.4 μm) clearly has its origin in the transverse nodal structure of the initial state that is formed upon laser excitation. We note that beyond a distance of 0.4 μm the calculation shows no significant changes.

A direct comparison of the experimental (solid line) and calculated (dashed line) results that is obtained by scaling the radial coordinate in the calculation, is shown to the right of the experimental results. Here a comparison of the measured radial probability distribution $P_{\mathrm{exp}}(R) = \int P(R, \alpha) R d\alpha$ [where $P(R, \alpha)$ represents the intensity distribution in the experimental image in polar coordinates R and α], and the calculated radial probability distribution $P_{\mathrm{calc}}(R) = R|\Psi_{\mathrm{calc}}(R, t)|^2$ is given, showing very satisfactory agreement and validating the assignment of the number of dark fringes as the parabolic quantum n_1. Observed differences between the experimental and calculated results may be due to differences in the experimental conditions and the assumptions made in the calculations (where the Stark states were excited using a 250 ps excitation pulse), imperfections in the experimental images, and possible smearing effects due to the finite lifetime of the excited Stark states.

A striking observation in the experiments is the pronounced difference between images recorded following resonant excitation of a quasibound Stark state and images recorded following nonresonant excitation of the ionization continuum. This is illustrated in Fig. 4, where a comparison is shown between the image for the $(n_1, n_2, m) = (2, 27, 0)$ state and two nonresonant images recorded 1.8 cm^{-1} below and 1.1 cm^{-1} above this resonance. Remarkably, the outermost ring in the on-resonance image extends significantly further radially than in the two surrounding images. In fact, when comparing the experimental results (triangles in the inset) to calculations using the classical method used in

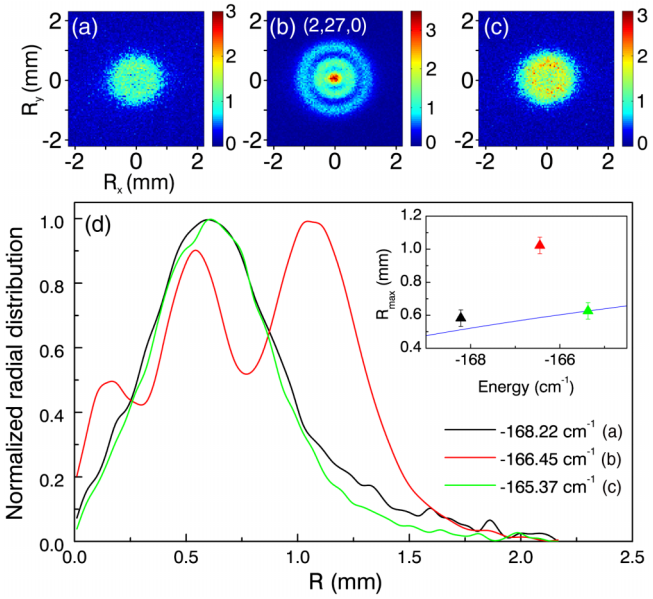

FIG. 4 (color online). Evidence for on-resonance ionization by tunneling through the Coulomb + static field potential. A comparison is shown between a measurement carried out for the $(n_1, n_2, m) = (2, 27, 0)$ resonance (b) and two non-resonant measurements performed 1.8 cm^{-1} below (a) and 1.1 cm^{-1} above (c) this resonance. The normalized radial distribution of the on- resonance measurement containing three maxima extends significantly further outward than the two off-resonance measurements which show only a single maximum (d). The inset in (d) shows a comparison of the radial extension of the experimental images, defined as the position of the outer maximum (color triangles) and the theoretical radial extension (blue, solid line) according to the classical formula (excluding tunneling contributions) $R_{\mathrm{max}} = [2L\frac{E-E_{sp}}{F}]^{1/2}$ [15], where L is the distance between the H atom and the detector ($L = 0.5$ m), and E_{sp} is the saddle point energy (-174.00 cm^{-1}). The experimental and theoretical radial extensions were matched for the measurement at $E = -165.37$ cm^{-1}.

Ref. [15] (solid blue line in the inset), one sees that the position of the outer ring in the image for the (2, 27, 0) resonance extends further outwards by about 70%. This is in line with recent theoretical work by Zhao and Delos, who developed both a semiclassical and a quantum-mechanical theory for the hydrogen atom photoionization microscopy problem [30,31]. They predicted a ''remarkable tunneling effect'' that applies *only* in the case of resonant excitation of quasibound Stark states. Classically, the electron is trapped by the potential barrier $V(\eta)$ [see Fig. 1(b)] if the emission angle is smaller than a critical angle $\theta_c = \arccos(1 - E^2/2F)$. However, in case of excitation to a quasibound state, electrons with an emission angle smaller than θ_c may tunnel through the $V(\eta)$ potential barrier, leading to a situation where the electron can reach a position on the detector that is not classically accessible.

Generally, the image measured at a resonance corresponds to a coherent superposition of resonant and

nonresonant contributions, the latter corresponding to direct excitation into the ionization continuum. As a consequence, a beating between these two contributions is expected. In the hydrogen measurements that are presented here, the resonant contribution strongly dominates. For example, the signal (i.e., the total number of detected electrons per acquisition) at the (2, 27, 0) resonance in Fig. 4 [case (b)] was stronger than the signal at the adjacent nonresonant positions [cases (a) and (c)] by a factor 10. Therefore, the image essentially represents a direct macroscopic projection of the microscopic electronic quantum state. In other atoms electron-electron interactions (as manifested by quantum defects) that couple the initial state (n_1, n_2, m) to other states have a major influence on the electronic wave that is observed. For example, the above-mentioning tunneling in the η coordinate is largely absent in nonhydrogenic systems, because (n_1, n_2, m) initial states that require tunneling couple to states that do not. In Xe, the coupling among parabolic states led to a complete disappearance of the resonant effects [16], whereas in Li it led to a substantial reduction of the contrast between resonant and nonresonant excitation [19].

In conclusion, we have shown that the concept of photoionization microscopy, as theoretically proposed more than 30 years ago and the subject of recent theoretical work predicting the possibility to experimentally observe nonclassical photoionization dynamics involving tunneling through the $V(\eta)$ potential barrier, can be experimentally realized, providing both a beautiful demonstration of the intricacies of quantum mechanics and a fruitful playground, where the fundamental implications of this theory can be further explored. For example, predictions have already been made for the case where both electric and magnetic fields are present [32]. The experimental observations of the nodal structures of the wave functions presented in this Letter are not specific to the field strengths and laser excitation conditions (i.e., the polarization direction of the exciting laser) used, but are a general phenomenon that is observable and can be exploited over a wide range of experimental conditions.

We acknowledge valuable contributions by Rob Kemper, Marco Konijnenburg, Iliya Cerjak, and Henk-Jan Boluijt. This work is part of the research program of the Stichting voor Fundamenteel Onderzoek der Materie (FOM), which is financially supported by the Nederlandse Organisatie voor Wetenschappelijk Onderzoek (NWO). Francis Robicheaux is supported by the U.S. Department of Energy.

*Corresponding author.

[1] E. Schrödinger, Phys. Rev. **28**, 1049 (1926).
[2] H. Wimmel, *Quantum Physics and Observed Reality: A Critical Interpretation of Quantum Mechanics* (World Scientific, Singapore, 1992).
[3] C. Jönsson, Z. Phys. A **161**, 454 (1961).
[4] L. D. Noordam and R. R. Jones, J. Mod. Opt. **44**, 2515 (1997).
[5] I. E. Mccarthy and E. Weigold, Rep. Prog. Phys. **51**, 299 (1988).
[6] J. Itatani, J. Levesque, D. Zeidler, H. Niikura, H. Pepin, J. C. Kieffer, P. B. Corkum, and D. M. Villeneuve, Nature (London) **432**, 867 (2004).
[7] D. Shafir, Y. Mairesse, D. M. Villeneuve, P. B. Corkum, and N. Dudovich, Nat. Phys. **5**, 412 (2009).
[8] Y. N. Demkov, V. D. Kondratovich, and V. N. Ostrovskii, JETP Lett. **34**, 403 (1981).
[9] V. D. Kondratovich and V. N. Ostrovsky, J. Phys. B **17**, 2011 (1984).
[10] V. D. Kondratovich and V. N. Ostrovsky, J. Phys. B **23**, 3785 (1990).
[11] L. D. Landau and E. M. Lifshitz, *Quantum Mechanics: Non-Relativistic Theory* (Pergamon, New York, 1965).
[12] T. F. Gallagher, *Rydberg Atoms* (Cambridge University Press, Cambridge, England, 1994).
[13] C. Blondel, C. Delsart, and F. Dulieu, Phys. Rev. Lett. **77**, 3755 (1996).
[14] M. L. Du, Phys. Rev. A **40**, 4983 (1989).
[15] C. Bordas, Phys. Rev. A **58**, 400 (1998).
[16] C. Nicole, H. L. Offerhaus, M. J. J. Vrakking, F. Lepine, and C. Bordas, Phys. Rev. Lett. **88**, 133001 (2002).
[17] C. Bordas, F. Lepine, C. Nicole, and M. J. J. Vrakking, Phys. Rev. A **68**, 012709 (2003).
[18] F. Lepine, C. Bordas, C. Nicole, and M. J. J. Vrakking, Phys. Rev. A **70**, 033417 (2004).
[19] S. Cohen, M. M. Harb, A. Ollagnier, F. Robicheaux, M. J. J. Vrakking, T. Barillot, F. Lépine, and C. Bordas [Phys. Rev. Lett. (to be published)].
[20] See Supplemental Material at http://link.aps.org/supplemental/10.1103/PhysRevLett.110.213001 for a detailed description of the experimental setup and of the wave packet approach used for solving the time-dependent Schrödinger equation.
[21] A. T. J. B. Eppink and D. H. Parker, Rev. Sci. Instrum. **68**, 3477 (1997).
[22] E. Cromwell, T. Trickl, Y. T. Lee, and A. H. Kung, Rev. Sci. Instrum. **60**, 2888 (1989).
[23] H. L. Offerhaus, C. Nicole, F. Lepine, C. Bordas, F. Rosca-Pruna, and M. J. J. Vrakking, Rev. Sci. Instrum. **72**, 3245 (2001).
[24] R. J. Damburg and V. V. Kolosov, J. Phys. B **12**, 2637 (1979).
[25] C. Delsart, L. Cabaret, C. Blondel, and R. J. Champeau, J. Phys. B **20**, 4699 (1987).
[26] P. M. Koch and D. R. Mariani, Phys. Rev. Lett. **46**, 1275 (1981).
[27] D. A. Harmin, Phys. Rev. A **24**, 2491 (1981).
[28] D. A. Harmin, Phys. Rev. A **26**, 2656 (1982).
[29] F. Robicheaux and J. Shaw, Phys. Rev. Lett. **77**, 4154 (1996).
[30] L. B. Zhao and J. B. Delos, Phys. Rev. A **81**, 053417 (2010).
[31] L. B. Zhao and J. B. Delos, Phys. Rev. A **81**, 053418 (2010).
[32] L. Wang, H. F. Yang, X. J. Liu, H. P. Liu, M. S. Zhan, and J. B. Delos, Phys. Rev. A **82**, 022514 (2010).